

The study of heat transfer and laminar flow of kerosene/multi-walled carbon nanotubes (MWCNTs) nanofluid in the microchannel heat sink with slip boundary condition

Abedin Arabpour¹ · Arash Karimipour² · Davood Toghraie¹

Received: 25 May 2017 / Accepted: 12 August 2017 / Published online: 4 September 2017
© Akadémiai Kiadó, Budapest, Hungary 2017

Abstract In this investigation, the laminar heat transfer of kerosene nanofluid/multi-walled carbon nanotubes in the microchannel heat sink is studied. The considered microchannel is two layers in which the length of bottom layer is truncated and is equal to the half of the length of bottom layer. The length of microchannel bottom layer is $L = 3$ mm, and the length of top layer is $L_1 = 1.5$ mm. The microchannel is made of silicon, and each layer of microchannel has the thickness of $t = 12.5$ μm . Along the external bottom wall, the sinusoidal oscillating heat flux is applied. The top external and lateral walls are insulated, and they do not have heat transfer with the environment. The results of this research revealed that in different Reynolds numbers, applying oscillating heat flux significantly influences the profile figure of Nusselt number and this impressionability is obvious in Reynolds numbers of 10 and 100. Also, by increasing the slip velocity coefficient on the solid surfaces, the amount of minimum temperature reduces significantly which behavior remarkably entails the heat transfer enhancement.

Keywords Heat transfer · Kerosene/multi-walled carbon nanotubes · Microchannel heat sink · Oscillating heat flux · Slip velocity coefficient

List of symbols

| | |
|-----------------------------|--|
| A | Area (m^2) |
| $B = \beta/H$ | Dimensionless slip velocity |
| C_f | Skin friction factor |
| C_p | Heat capacity ($\text{J kg}^{-1} \text{K}^{-1}$) |
| H | Microchannel height (m) |
| K | Thermal conductivity coefficient ($\text{W m}^{-1} \text{K}^{-1}$) |
| L | Down-layer microchannel length (m) |
| L_1 | Top-layer microchannel length (m) |
| Nu | Nusselt number |
| P | Fluid pressure (Pa) |
| $Pe = (u_s d_s / \alpha_f)$ | Peclet number |
| $Pr = \nu_f / \alpha_f$ | Prandtl number |
| $q''(X)$ | Oscillating heat flux (W m^{-2}) |
| q_0'' | Constant heat flux (W m^{-2}) |
| R | Thermal resistance (K W^{-1}) |
| $Re = \rho_f u_c d / \mu_f$ | Reynolds number |
| T | Temperature (K) |
| $(U, V) = (u/U_0, v/U_0)$ | Dimensionless velocity components in x, y directions |
| $(X, Y) = (x/d, y/d)$ | Cartesian dimensionless coordinates |
| u, v | Velocity components in x, y directions (m s^{-1}) |
| u_c (m/s) | Inlet velocity in x directions (m s^{-1}) |
| u_s (m/s) | Brownian motion velocity (m s^{-1}) |

✉ Arash Karimipour
arashkarimipour@gmail.com

¹ Department of Mechanical Engineering, Khomeinishahr Branch, Islamic Azad University, Khomeinishahr, Iran

² Department of Mechanical Engineering, Najafabad Branch, Islamic Azad University, Najafabad, Iran

Greek symbols

| | |
|---------|-------------------------------|
| β | Slip velocity coefficient (m) |
| ϕ | Nanoparticles volume fraction |

| | |
|-------------------------------|--|
| $\lambda_1 = L_1/L$ | Dimensionless length ration |
| μ | Dynamic viscosity (Pa s ⁻¹) |
| $\theta = (T - T_C)/\Delta T$ | Dimensionless temperature |
| ρ | Density (kg m ⁻³) |
| τ | Shear stress (N m ⁻²) |
| ν | Kinematics viscosity (m ² s ⁻¹) |

Super- and subscripts

| | |
|-----|-------------------------|
| Ave | Average |
| c | Cold |
| Eff | Effective |
| f | Base fluid (pure water) |
| H | Hot |
| In | Inlet |
| Max | Maximum |
| Min | Minimum |
| nf | Nanofluid |
| Out | Outlet |
| S | Solid nanoparticles |

Introduction

The cooling of miniature equipment in the micro electro mechanical and nano-electromechanical industries has increased the need of understanding the fluid flow and heat transfer in the micro- and nanogeometries. The behavior of fluid flow and heat transfer in the miniature scales and by using nanofluid, due to the improvement in heat transfer mechanisms in nano- and microdimensions, comparing to the custom scales, is far different. Numerous numerical and empirical studies have been done for investigating the flow and heat transfer of custom fluids and nanofluid in the microchannels whose main purpose is increasing the heat transfer [1–5]. The investigation of heat transfer enhancement in different industrial and experimental fluids by using novel methods has been expanded as the study fields among the adherents of this issue [6]. The microchannel heat sink as an applicable miniature equipment has high importance in heat transfer of electronic industries. This equipment has been suggested by Tukerman and Pease [7] for cooling the electronic chips. In recent decades, this equipment has been investigated and optimized by researchers in different structures and arrangements for enhancing the cooling of electronic chips [8–10]. Kulkarni et al. [11] numerically studied the multi-purposed optimization of double-layer microchannel heat sink with the cross-figured inlet section. Their results evidenced that the microchannel with narrower design has lower thermal resistance and higher pumping power and the pumping power by increasing the heat flux reduces significantly. Husain and Kim [12, 13] optimized the indented

microchannel heat sink and indicated that the thermal resistance of microchannel heat sink by optimization reduces considerably. Xie et al. [14] studied the efficiency of double-layer microchannel heat sink with the wavy wall in the states of parallel and contrary flows. They investigated the effects of wavy wall limitation and the ratio of mass flow on the thermal resistance and pressure drop parameters. Seyf and Nikaein [15] by using Al₂O₃, zinc and Cu nanoparticles in the ethylene glycol/water fluid numerically studied the effects of nanoparticles dimensions and Brownian motion of nanoparticles on the thermal performance of a rectangular microchannel heat sink. Their results showed that the amount of nanofluid conductivity without considering the Brownian motion reduces almost to 6.5%. Wu et al. [16] numerically studied the thermal resistance, pumping power and thermal distribution on the wall surface of double-layer microchannel heat sink (DL-MCHS). In their research, different parameters of microchannel dimensions and different flow conditions have been studied. The results of his study showed that the improvement in total efficiency of double-layer microchannel heat sink depends on the pumping power. Chen and Chung [17] used the water/Cu nanofluid. In their investigation, the absorbed energy by the nanofluid was more than the absorbed energy by water, and it has been observed that by enhancing volume fraction of nanoparticles, the high-temperature differences accomplish between the inlet and outlet sections of microchannel heat sink in a low flow rate. Jang and Choi [18] by using nanofluid numerically studied the cooling performance of a microchannel heat sink. They reported that the nanofluid causes the reduction in thermal resistance and dimensionless temperature difference in microchannel heated wall and cooling fluid. Sui et al. [19] numerically investigated the fluid flow in the wavy microchannels. Their numerical results indicated that with the uniform cross section, the thermal performance of wavy microchannel is higher than the rectangular flat one. Ho et al. [20] studied the forced convection cooling performance of a Copper microchannel heat sink with water/Al₂O₃ nanofluid as the cooling fluid. Their results showed that the heat sink cooled by nanofluid, comparing to the heat sink cooled by water, has more average heat transfer coefficient. Till now, numerous researches about the heat transfer in the microchannels and nanofluid have been presented, and sometimes, the slip velocity conditions, the effects of magnetic field and the forced heat transfer under the influence of constant temperature or constant heat flux have been investigated separately [21–35]. Nikkhah et al. [36] numerically studied the water nanofluid/functional multi-walled carbon nanotubes in a two-dimensional microchannel with slip and no-slip boundary conditions. They concluded that the augment of solid nanoparticles weight fraction and slip

velocity coefficient cause the increase in Nusselt number, and in higher Reynolds numbers, this enhancement is more considerable. In their research, the computational fluid dynamics and laminar heat transfer of kerosene nanofluid/multi-walled carbon nanotubes in the double-layer microchannel heat sink are simulated in the two-dimensional domain. By considering the effect of slip boundary condition on the outcome results of numerical simulation, in this study, the slip velocity boundary condition on the solid walls is used. The results of this research are presented for different volume fractions of nanoparticles, slip velocity coefficients and different ranges of Reynolds numbers. The main purpose of this study is investigating the behavior of temperature domain and hydrodynamic of laminar flow of nanofluid in the two-dimensional double-layer microchannel.

Problem statement

In the present study, the laminar flow of kerosene nanofluid/multi-walled carbon nano tubes in volume fractions of 0, 4 and 8% of nanoparticles is investigated. Figure 1 indicates the studied geometrics of this paper. In this research, the material of microchannel is silicon. In Fig. 1, the bottom layer of microchannel is $L = 3$ mm and the height is $H = 50 \mu\text{m}$. The top layer of microchannel with the length of L_2 is equal to $L_2 = 1.5$ mm, and by placing on the bottom layer at the interface area, the heat transfers with it and in this region, the amount of heat generation is constant and is equal to 100 kw/m^3 . In each layer of microchannel, the silicon material with the thickness of $t = 12.5 \mu\text{m}$ has surrounded the layers. The external areas of top layer with the length of L_2 are insulated, and the bottom area of microchannel, on the external wall with the length of L , is under the influence of sinusoidal flux with the equation of $q''(X) = 2q_0'' + q_0'' \sin(\frac{\pi X}{4})$ in which the amount is calculated from the equation of (q_0'') . With the definition of dimensionless slip velocity coefficient as

$(B = \beta/H)$, the ratio of slip velocity coefficient to the height of microchannel, in this research, the numerical simulation is done for the dimensionless slip velocity coefficients $(B = \beta/H)$ of 0.001, 0.01 and 0.1 and Reynolds numbers of 1, 10 and 100. The inlet fluid at the top and bottom layers enters with the temperature of 301 K as shown in Fig. 1. All of the internal walls which are in contact with fluid have the slip velocity boundary condition. The used nanofluid properties of this simulation and the material of microchannel wall are described, respectively, in Table 1.

In this simulation, the fluid flow and heat transfer are considered as laminar and fully developed. The nanofluid properties are considered as constant and independent from the temperature. The solid-liquid suspension in less densities is modeled as single-phased, and on the channel walls, the oscillating heat flux is applied. The slip boundary condition is used on the microchannel. The numerical simulation domain is two dimensional.

Governing equations

The dimensionless governing equations on the simulation domain are defined as follows [39, 40]:

Continuity equation:

$$U \frac{\partial U}{\partial X} + V \frac{\partial V}{\partial Y} = 0 \tag{1}$$

Momentum equation:

$$U \frac{\partial U}{\partial X} + V \frac{\partial U}{\partial Y} = -\frac{\partial P}{\partial X} + \frac{\mu_{nf}}{\rho_{nf} \nu_f} \frac{1}{Re} \left(\frac{\partial^2 U}{\partial X^2} + \frac{\partial^2 U}{\partial Y^2} \right) \tag{2}$$

$$U \frac{\partial V}{\partial X} + V \frac{\partial V}{\partial Y} = -\frac{\partial P}{\partial Y} + \frac{\mu_{nf}}{\rho_{nf} \nu_f} \frac{1}{Re} \left(\frac{\partial^2 V}{\partial X^2} + \frac{\partial^2 V}{\partial Y^2} \right) \tag{3}$$

Energy equation:

$$U \frac{\partial \theta}{\partial X} + V \frac{\partial \theta}{\partial Y} = \frac{\mu_{nf}}{\alpha_f} \frac{1}{Re Pr} \left(\frac{\partial^2 \theta}{\partial X^2} + \frac{\partial^2 \theta}{\partial Y^2} \right) \tag{4}$$

For non-dimensionalizing Eqs. (1)–(4), following parameters are used [36]:

Table 1 The thermophysical properties of base fluid and nanoparticle of multi-walled carbon nanotubes and silicon [37, 38]

| $\phi/\%$ | $\rho/$ kg m^{-3} | $C_p/$ $\text{J kg}^{-1} \text{K}^{-1}$ | $k/$ $\text{W m}^{-1} \text{K}^{-1}$ | $\mu/\text{Pa s}$ | Pr |
|-----------|-------------------------------|--|---|-------------------|------|
| 0 | 783 | 2090 | 0.145 | 0.001457 | 21 |
| 4 | 815 | 1989 | 0.265 | 0.001613 | 12.1 |
| 8 | 845 | 1895 | 0.390 | 0.001795 | 8.72 |
| Silicon | 2329 | 702 | 124 | – | – |

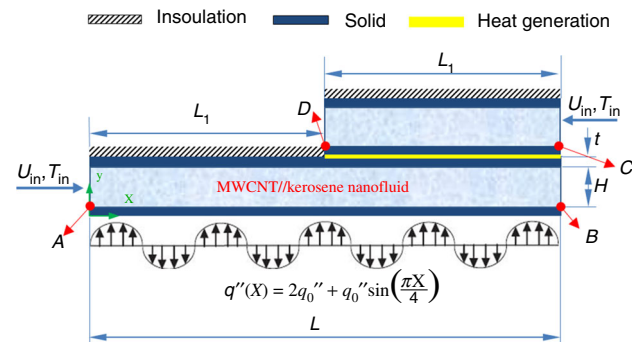


Fig. 1 The studied schematics of this research

$$\begin{aligned}
 X &= \frac{x}{H} & Y &= \frac{y}{H} & V &= \frac{v}{u_c} \\
 \theta &= \frac{T - T_c}{\Delta T} & U &= \frac{v}{u_c} & B &= \frac{\beta}{H} \\
 \Delta T &= \frac{q_0'' H}{k_f} & Pr &= \frac{v_f}{\alpha_f} & P &= \frac{\bar{P}}{\rho_{nf} u_c^2}
 \end{aligned}
 \tag{5}$$

Another parameter for investigating the microchannel performance is the friction coefficient which is calculated from the following equation [41]:

$$C_f = \frac{2 \times \tau_w}{\rho u_{in}^2} \tag{6}$$

The average Nusselt number can be obtained as follows [42, 43]:

$$Nu_x = \frac{h \times H}{k_f} \rightarrow Nu_{ave} = \frac{1}{L} \int_0^L Nu_x(X) dX \tag{7}$$

The amounts of thermal resistance [44, 45] of bottom wall of microchannel and pressure drop are calculated from the following equation:

$$\begin{aligned}
 R &= \frac{T_{max} - T_{min}}{q_0'' \times A} = \frac{T_{max} - T_{in}}{q_0'' \times A} \rightarrow A = W \times L \rightarrow R \times W \\
 &= \frac{T_{max} - T_{min}}{q_0'' \times L}
 \end{aligned}
 \tag{8}$$

$$\Delta P = P_{in} - P_{out} \tag{9}$$

In Eq. (9), T_{max} , T_{min} , A and q_0'' are, respectively, the maximum temperature of bottom wall, the minimum temperature (the temperature of inlet fluid), cross section and the applied heat flux to the AB wall.

The governing boundary conditions on the problem-solving

The hydrodynamic and thermal boundary conditions used in this problem are as follows:

Table 2 The changes in studied grid numbers in the present study

| Re | Parameters | Grid point | | | |
|----------|---------------|------------|---------|----------|-----------|
| | | 30,000 | 50,000 | 63,000 | 100,000 |
| Re = 100 | Nu_{ave} | 9.786 | 10.2103 | 10.4661 | 10.623 |
| | Error | 7.9% | 3.89% | 1.48% | Base grid |
| | $\Delta P/Pa$ | 101,231 | 97,635 | 94,908.5 | 94,851 |
| | Error% | 6.72% | 2.94% | 0.06% | Base grid |
| Re = 10 | Nu_{ave} | 3.68 | 4.011 | 4.0248 | 4.101 |
| | Error | 10.27% | 2.2% | 1.86% | Base grid |
| | $\Delta P/Pa$ | 9845 | 9271 | 9161.3 | 9100.5 |
| | Error | 8.2% | 1.88% | 0.67% | Base grid |

$$\begin{aligned}
 &U = 1, \quad V = 0 \quad \text{and} \quad \theta = 0 \quad \text{for} \quad X = 0 \quad \text{and} \\
 &0.25 \leq Y \leq 1.25 \quad \text{and} \quad X = 60, \quad 1.75 \leq Y \leq 2.75 \\
 &V = 0 \quad \text{and} \quad \frac{\partial \theta}{\partial X} = \frac{\partial U}{\partial X} \quad \text{for} \quad X = 60 \quad \text{and} \\
 &0.25 \leq Y \leq 1.25 \quad \text{and} \quad X = 30, \quad 1.75 \leq Y \leq 2.75 \\
 &V = 0, \quad U = 0 \quad \text{and} \quad \frac{\partial \theta}{\partial Y} = 2q_0'' + q_0'' \sin\left(\frac{\pi X}{4}\right) \\
 &\text{for} \quad Y = 0 \quad \text{and} \quad 0 \leq X \leq 60 \\
 &V = 0, \quad U_s = B \frac{\partial \theta}{\partial Y} \quad \text{and} \quad k_{nf} \frac{\partial \theta}{\partial Y} = k_s \frac{\partial \theta}{\partial Y} \\
 &\text{for} \quad Y = 0.25 \quad \text{and} \quad 0 \leq X \leq 60 \\
 &V = 0, \quad U = 0 \quad \text{and} \quad \frac{\partial \theta}{\partial Y} = 0 \quad \text{for} \quad Y = 1.5 \quad \text{and} \\
 &0 \leq X \leq 30 \quad \text{and} \quad Y = 3 \quad \text{and} \quad 0 \leq X \leq 60 \\
 &V = 0, \quad U_s = B \frac{\partial U}{\partial Y} \quad \text{and} \quad k_{nf} \frac{\partial \theta}{\partial Y} = k_s \frac{\partial \theta}{\partial Y} \quad \text{for} \\
 &Y = 1.25 \quad \text{and} \quad 0 \leq X \leq 60 \\
 &V = 0, \quad -U_s = B \frac{\partial U}{\partial Y} \quad \text{and} \quad k_{nf} \frac{\partial \theta}{\partial Y} = k_s \frac{\partial \theta}{\partial Y} \quad \text{for} \\
 &Y = 1.75 \quad \text{and} \quad 30 \leq X \leq 60 \\
 &V = 0, \quad -U_s = B \frac{\partial U}{\partial Y} \quad \text{and} \quad k_{nf} \frac{\partial \theta}{\partial Y} = k_s \frac{\partial \theta}{\partial Y} \quad \text{for} \\
 &Y = 2.75 \quad \text{and} \quad 30 \leq X \leq 60
 \end{aligned}
 \tag{10}$$

The mesh study and numerical solving procedure

In order to ensure the results independency of this research, the rectangular organized grids have changed from the number of 30,000 to 100,000. The studied parameters in the validation of present investigation are including Nusselt number along the AB wall and the amount of pressure drop. The changes in these two parameters are investigated in Reynolds numbers of 10 and 100 and volume fraction of 8% of nanoparticles in the slip velocity coefficient of 0.01. According to Table 2, by choosing grid number of 100,000, comparing to other grid numbers, more accurate results can be obtained. However, the grid number of 63,000, compared to the grid number of 100,000, has acceptable error and less demanded time for solving the numerical domain; therefore, in this numerical simulation, the grid number of 63,000 has been used. In this study, in order to enhance the solving accuracy, to couple velocity and pressure, SIMPLEC algorithm [46, 47] has been used, and the maximum loss for results convergence of this simulation has been chosen 10^{-6} [48–50].

Results and discussion

Validation

The results of the present study have been validated with the numerical study of Nikkhah et al. [36] in Reynolds number of 100 for the dimensionless temperature parameter at central section of flow. Nikkhah et al. [36] numerically investigated the laminar flow and heat transfer of water nanofluid/functional carbon nanotubes in a rectangular microchannel with the ratio of length to the height of channel equal to 32. Their investigation has been done in Reynolds numbers of 1–100 for volume fractions of

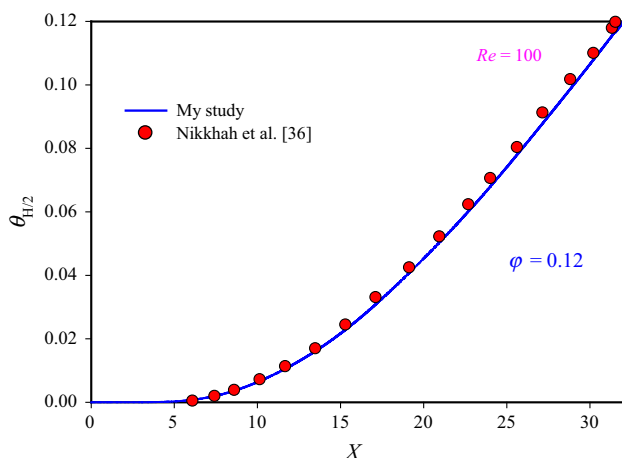


Fig. 2 The validation with numerical study of Nikkhah et al. [36]

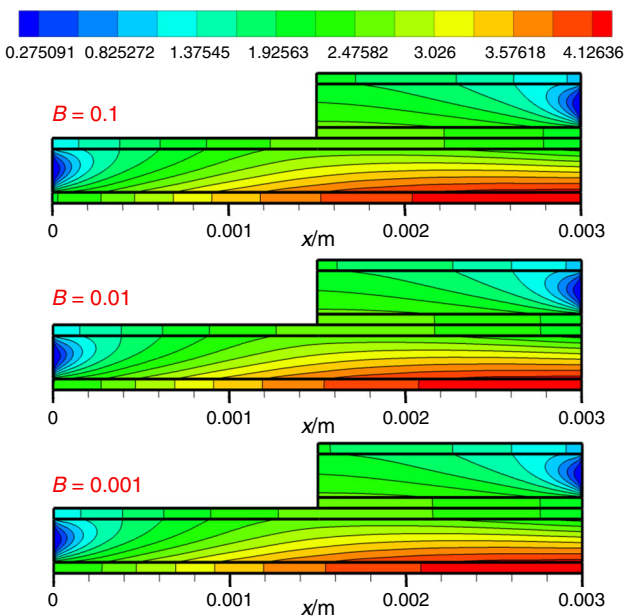


Fig. 3 The changes in dimensionless temperature in Reynolds number of 1 and different dimensionless slip coefficients in volume fraction of 0%

0–0.25% of nanoparticles. According to Fig. 2 and proper coincidence of the results of the present research with the study of Nikkhah et al. [36], it can be said that the solving procedure and the applied boundary conditions are accurate.

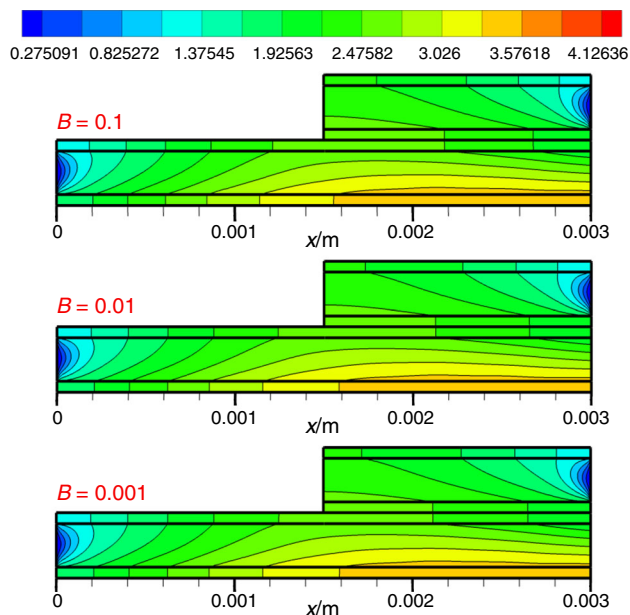


Fig. 4 The changes in dimensionless temperature in Reynolds number of 1 and different dimensionless slip coefficients in volume fraction of 4%

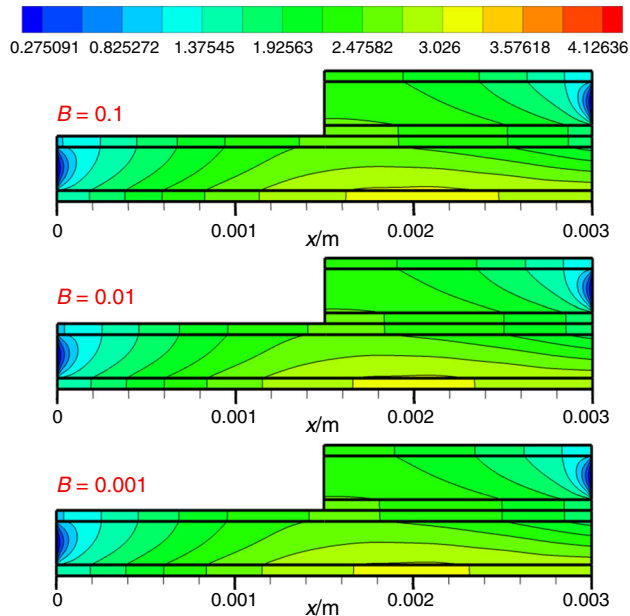


Fig. 5 The changes in dimensionless temperature in Reynolds number of 1 and different dimensionless slip coefficients in volume fraction of 8%

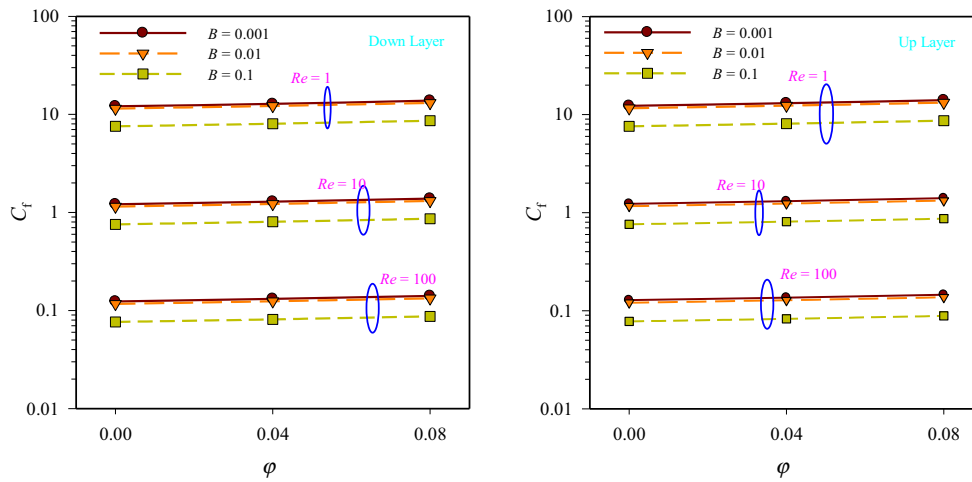
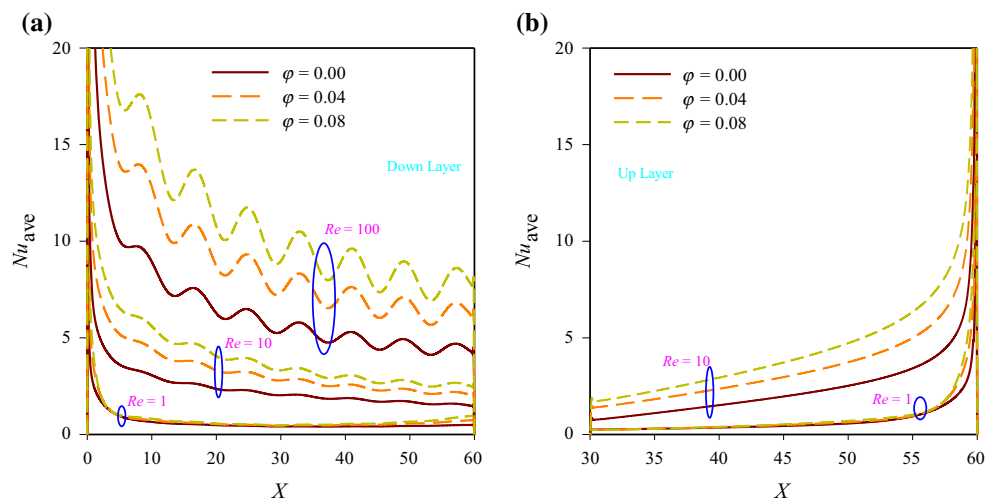


Fig. 6 The amount of average friction coefficient for the bottom and top layers, respectively, along the walls of (AB) and (CD)

Fig. 7 The amounts of average Nusselt number for the bottom and top layers, respectively, along the walls of (AB) and (CD)



Figures 3–5 demonstrate the dimensionless temperature contours in Reynolds number of 1, volume fractions of 0–8% of nanoparticles and different dimensionless slip coefficients at the dimensionless length of 1.2. By entering the fluid to the microchannel, by considering the maximum temperature of surface and fluid, the most changes in dimensionless temperature arise in this region. By more processing of fluid, due to the contact with hot surface on the direction of fluid motion in the microchannel, the changes in dimensionless temperature enhance in a way that this augment of dimensionless temperature causes the reduction in heat transfer and enhancement of hot areas in the microchannel. Due to the generation of uniform heat between the top and bottom layers of microchannel, this factor influences the top and bottom areas of microchannel. According to the existence of hot areas in the top layer of microchannel and increase in the dimensionless temperature in this area, the heat transfer reduces in these regions. The amount of dimensionless temperature changes and the

existence of hot area at the bottom layers are completely obvious from the middle area of microchannel to the lateral in Reynolds number of 1 and volume fraction of 0%. In all figures, by enhancing the dimensionless slip velocity coefficient and volume fraction, the elimination of hot areas at the top and bottom layers has been approximately solved.

Figure 6 illustrates the average friction coefficient for the bottom and top layers, respectively, along the walls of (AB) and (CD). This study has been done for dimensionless slip velocity coefficient of 0.001–0.1 in volume fractions of 0–8% of nanoparticles in Reynolds numbers of 1, 10 and 100. By enhancing Reynolds number, the contact of surface and fluid reduces which causes the reduction in friction coefficient. By increasing volume fraction of nanoparticles, due to the enhancement of viscosity and density of cooling fluid, the average friction coefficient increases. By augmenting the dimensionless slip velocity coefficient, due to the movement of fluid with less

Fig. 8 The changes in static pressure along the microchannel center in top and bottom layers

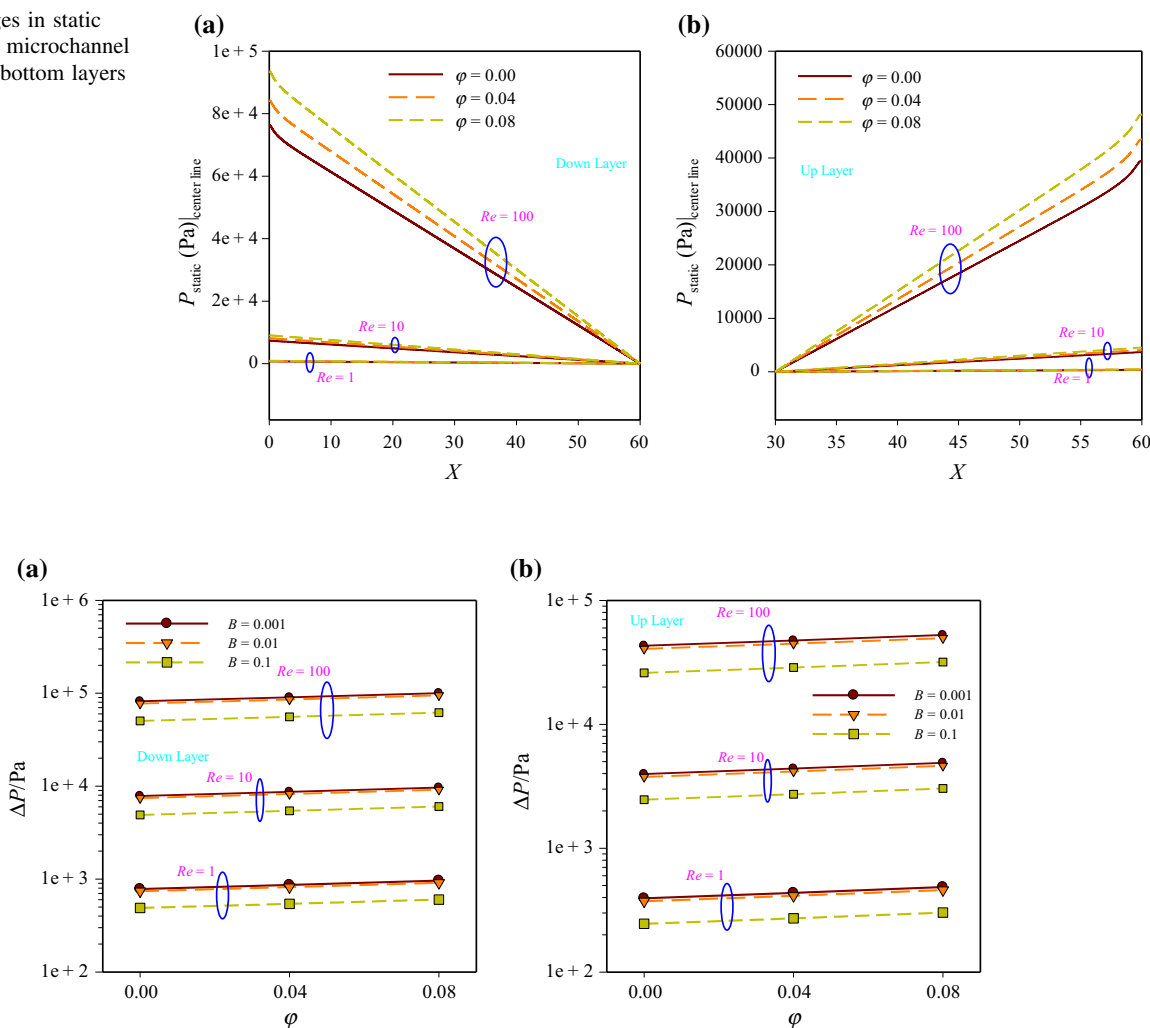


Fig. 9 The pressure drop for **a** bottom layer and **b** the top layer

resistance and depreciation on the surface, the friction coefficient decreases significantly. In each of the studied Reynolds numbers, the amount of average friction coefficient in Reynolds number of 1 is remarkable. In Reynolds numbers of 10 and 100, this factor decreases considerably. In the investigation of the amount of average friction coefficient at the top and bottom layers of microchannel, it can be said that comparing the top layer of microchannel to the bottom layer in volume fraction and Reynolds number and dimensionless slip velocity in the same conditions, the amount of average friction coefficient is more. This behavior is due to the enhancement of velocity gradients at the top layer comparing to the bottom layer.

Figure 7 shows the local Nusselt number for the bottom layer (a) and top layer (b), respectively, along the walls of (AB) and (CD). This study has been investigated for the slip velocity coefficient of 0.1, Reynolds numbers of 1–100 at the bottom layer and Reynolds numbers of 1–10 at the top layer and volume fractions of 0–8%. By

increasing Reynolds number, the local Nusselt number enhances. According to the increase in thermal conductivity coefficient of nanofluid, by enhancing volume fraction and the heat transfer, Nusselt number enhances. The other reason of this augmentation of Nusselt number in higher volume fractions is due to the acceleration of energy exchanging process in fluid because of the random movement of nanoparticles inside it. This process causes more uniform temperature distribution inside the nanofluid, and consequently, the rate of heat transfer between the wall and nanofluid increases. Because the fluid is only conductor heat flux between the upper- and down-layer microchannels, and since heat flux penetrates into all layers of fluid and is mixed during the movement of the fluid, therefore, the oscillatory shape of the heat flux is gone and the heat flux reaches the top layer uniformly. Hence, the shape of the Nusselt number diagrams in the upper layer does not depend on the oscillatory shape of the heat flux.

Fig. 10 The changes in maximum temperature at the bottom layer of microchannel along the wall of (AB)

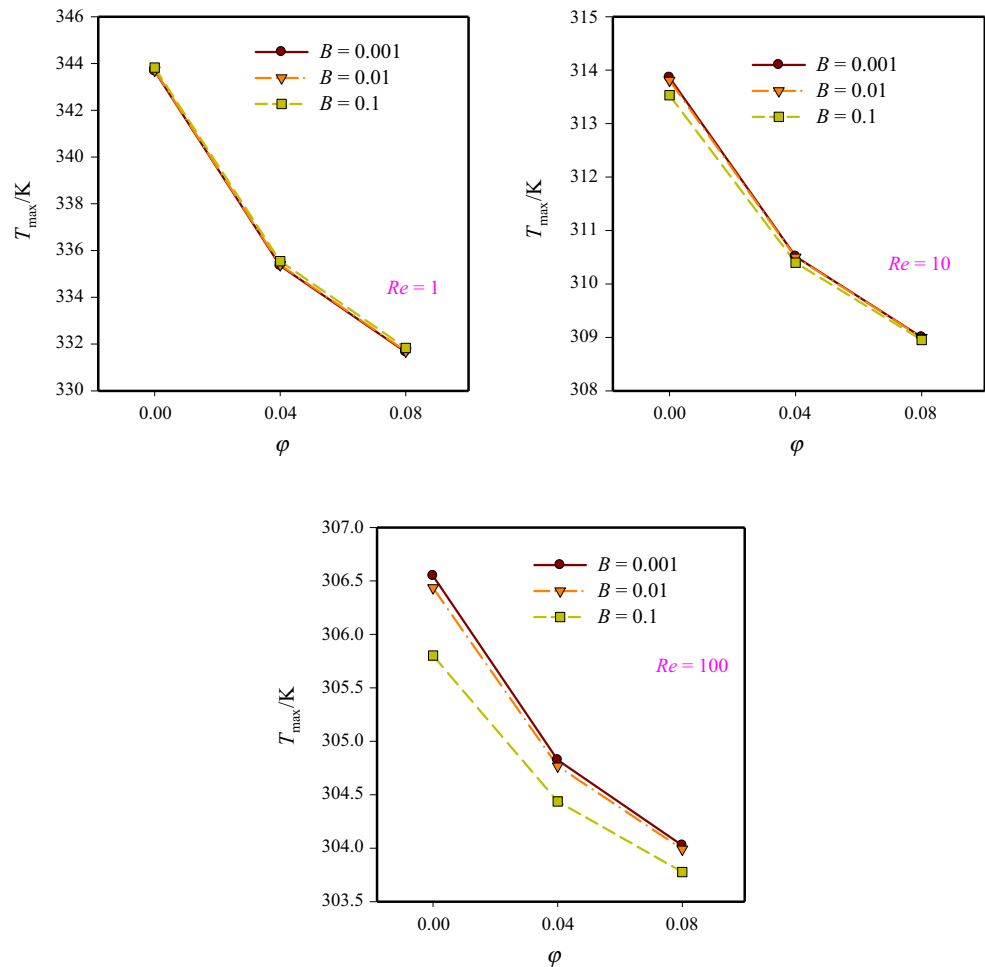


Figure 8 demonstrates the changes in static pressure for the bottom layer (a) and top layer (b) along the central line of flow in the dimensionless slip coefficient of 0.01. According to the figures, the amounts of pressure changing continue from the inlet section of microchannel to the outlet section. In the investigation of this parameter, it can be observed that the amounts of pressure changing at the top layer are less than at the bottom layer which is due to the reduction in the length of top channel comparing to the bottom channel. By increasing volume fraction of nanoparticles, due to the enhancement of particles number and density and viscosity of cooling fluid, the amount of static pressure on the direction of movement decreases more than the base fluid. By enhancing the slip velocity coefficient, the penetration of the effect of solid wall in the microchannel boundaries to the central core of flow reduces; therefore, by increasing the slip velocity coefficient, the amount of pressure drop decreases. According to Fig. 9, the minimum amount of pressure drop for the base fluid in slip velocity coefficient of 0.1 can be observed in each Reynolds number.

Figure 10 indicates the changes in average maximum temperature at the bottom layer of microchannel along the wall of (AB) in volume fractions of 0–8% for Reynolds numbers of 1, 10 and 100 for different slip velocity coefficients. The reduction in maximum temperature of surface is tantamount with better thermal removal from the hot surface. Among the studied states, the minimum amount of this parameter accomplishes in the highest fluid velocity and volume fraction. The effect of dimensionless slip velocity coefficient on the reduction in maximum temperature is considerable, in a way that in the dimensionless slip velocity coefficient of 0.1, comparing to the states of 0.001 and 0.01 has remarkable reduction. According to these figures, by increasing Reynolds number and volume fraction of nanoparticles and due to better mixture of fluid flow and heat transfer enhancement and increase in convection heat transfer coefficient, the maximum temperature factor reduces.

Figure 11 shows the changes in minimum temperature at the bottom layer of microchannel along the wall of (AB). According to the figures, the minimum temperature of

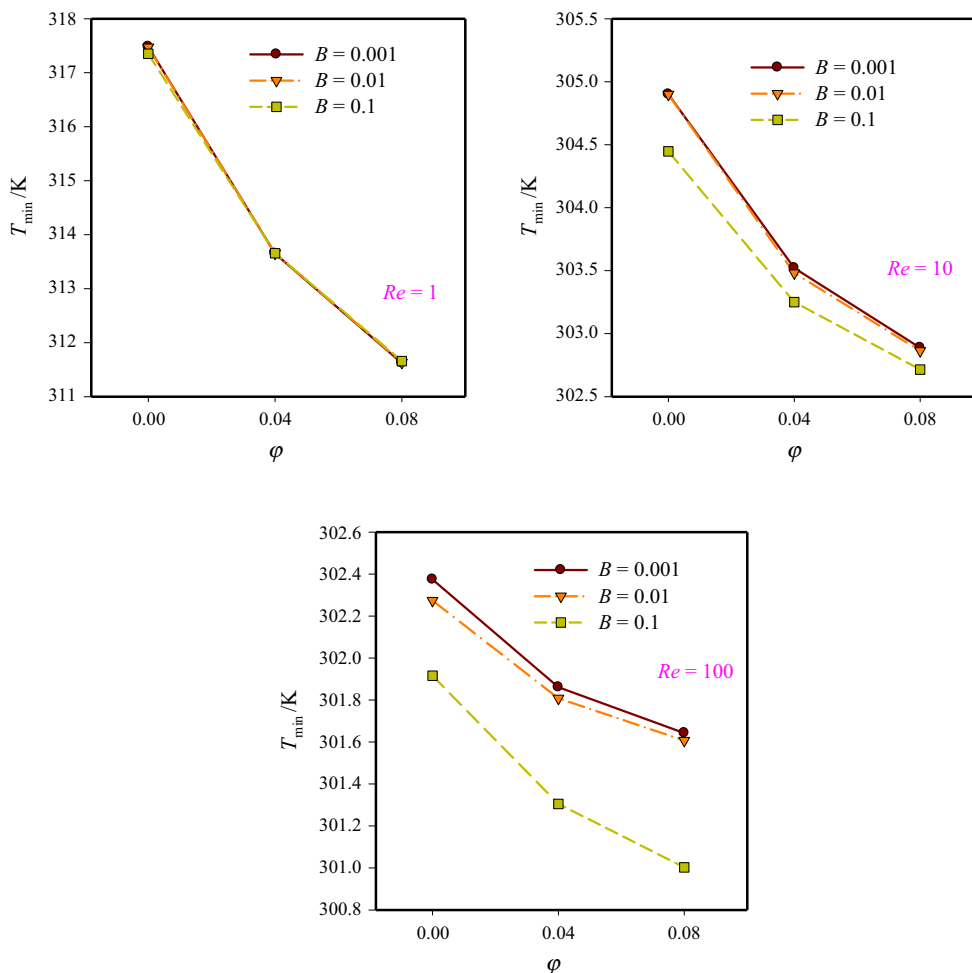


Fig. 11 The changes in minimum temperature at the bottom layer of microchannel along the wall of (AB)

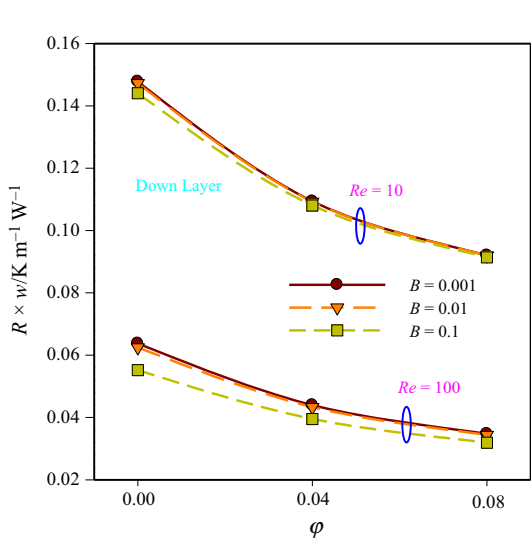


Fig. 12 The changes in thermal resistance at the bottom layer of microchannel along the wall of (AB)

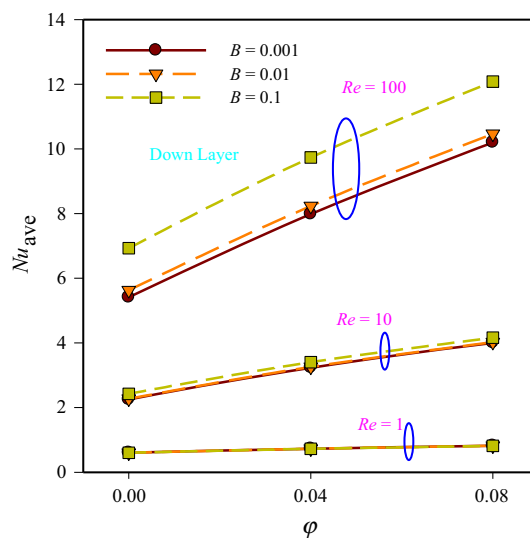
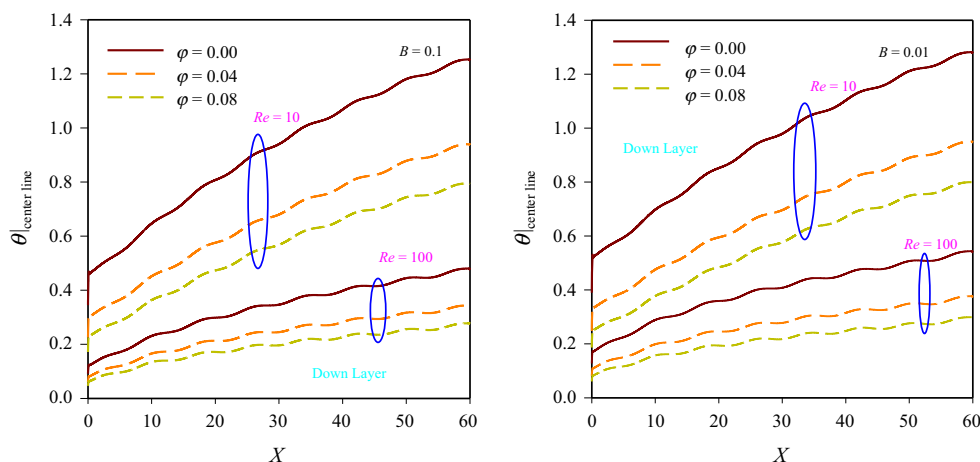


Fig. 13 The changes in average Nusselt number at the bottom layer of microchannel along the wall of (AB)

Fig. 14 The changes in dimensionless temperature at the bottom layer of microchannel along the wall of (AB)



surface accomplishes in a state in which the fluid has the highest heat transfer. The changes in this factor are the same as the changes in maximum temperature, and the reduction in minimum temperature entails the heat transfer enhancement.

Figure 12 illustrates the changes in thermal resistance at the bottom layer of microchannel along the wall of (AB) in Reynolds numbers of 10 and 100 in different volume fractions and the dimensionless slip velocity coefficient. This factor investigates the amount of maximum and minimum differences (the temperature of inlet fluid) of bottom layer of microchannel wall. The enhancement of dimensionless slip velocity coefficient causes the reduction in thermal resistance which entails the increase in heat transfer. In the studied Reynolds numbers of this research and in all considered factors, the increase in Reynolds number and in all considered factors, the increase in Reynolds number and volume fraction of nanoparticles causes the reduction in thermal resistance. With the increase in the fluid velocity (Reynolds number), the amount of heat transfer increases; due to an increase in the heat transfer coefficient, the maximum of surface temperature will reduce. By increasing the slip speed, the fluid moves with less deterrence on solid surfaces. As a result, the temperature of the hot surfaces is better transferred and the thermal resistance is reduced.

Figure 13 shows the changes in average Nusselt number at the bottom layer of microchannel along the wall of (AB). According to the amount of heat transfer in the investigated microchannel under the influence of velocity and volume fraction and different dimensionless slip velocity coefficients, it can be seen that the maximum amount of average Nusselt number arises in Reynolds number of 100. In the studied Reynolds numbers, the amount of heat transfer increases between 1.5 and 2.5 times.

Figure 14 illustrates the changes in dimensionless temperature at the bottom layer of microchannel along the wall of (AB) for the dimensionless slip velocity coefficients of

0.01 and 0.1. This investigation describes the differences in dimensionless temperature in different volume fractions and Reynolds numbers and the effect of slip length on this parameter. The reduction in dimensionless temperature on the hot wall is tantamount with heat transfer enhancement. It can be concluded from Fig. 14, the augment of Reynolds number and volume fraction of nanoparticles at the bottom layer of microchannel, the amount of dimensionless temperature reduces significantly.

Conclusions

In this research, the numerical simulation of laminar heat transfer of kerosene nanofluid/multi-walled carbon nanotubes in the microchannel heat sink by using finite volume method has been investigated. The results evidenced that in different Reynolds numbers, applying oscillating heat flux considerably influences the profile figure of Nusselt number, and this impressionability is obvious in Reynolds numbers of 100 and 10. Also, by enhancing the slip velocity coefficient on the solid surfaces, the amount of minimum temperature of surface decreases significantly which causes remarkable increase in heat transfer. According to the existence of hot area at the top layer of microchannel and increase in dimensionless temperature in this region, the heat transfer of this area reduces. By enhancing the dimensionless slip velocity coefficient, because the fluid moves on the surface with less resistance and depreciation, the friction coefficient decreases remarkably. In each of the studied Reynolds numbers, the amount of average friction coefficients in Reynolds number of 1 is more significant. By increasing Reynolds number and volume fraction of nanoparticles and due to better mixture of fluid flow and heat transfer enhancement and augmentation of convection heat transfer, the maximum temperature factor reduces. The increase in dimensionless

slip velocity coefficient entails the reduction in thermal resistance which causes the enhancement of heat transfer amount. Eventually, existence of incomplete upper layer on microchannel, due to the short path of fluid flow and lack of fully development fluid flow, better control of the down-layer temperature and increased heat transfer in microchannel, is created. It is recommended that in order to better distribute the temperature in a single-layer microchannel, the form of two-layer microchannel with incomplete upper layer is used. The extension of this paper for nanofluid according to previous works [51–113] affords engineers a good option for nanoscale and microscale simulation. According to some previous studies, to increase the produced power in some power plants, or to some upgrading, there is an emergency need to increase the heat transfer capacity in existing systems [114–120]. One of the best solutions for this problem is using nanofluids instead of water in these cooling systems.

References

- Togun H, Safaei MR, Sadri R, Kazi SN, Badarudin A, Hooman K, Sadeghinezhad E. Numerical simulation of laminar to turbulent nanofluid flow and heat transfer over a backward-facing step. *Appl Math Comput*. 2014;239:153–70.
- Yarmand H, Ahmadi G, Gharehkhani S, Kazi SN, Safaei MR, Alehashem MS, Mahat AB. Entropy generation during turbulent flow of zirconia–water and other nanofluids in a square cross section tube with a constant heat flux. *Entropy*. 2014;16:6116–32.
- Bashirnezhad K, Bazri S, Safaei MR, Goodarzi M, Dahari M, Mahian O, Wongwises S. Viscosity of nanofluids: a review of recent experimental studies. *Int Commun Heat Mass Transf*. 2016;73:114–23.
- Goodarzi M, Safaei MR, Vafai K, Ahmadi G, Dahari M, Kazi SN, Jomhari N. Investigation of nanofluid mixed convection in a shallow cavity using a two-phase mixture model. *Int J Therm Sci*. 2014;75:204–20.
- Hassan M, Sadri R, Ahmadi G, Dahari MB, Kazi SN, Safaei MR, Sadeghinezhad E. Numerical study of entropy generation in a flowing nanofluid used in micro-and minichannels. *Entropy*. 2013;15:144–55.
- Murshed SMS, Leong KC, Yang C. Thermophysical and electrokinetic properties of nanofluids: a critical review. *Appl Therm Eng*. 2008;28:2109–25.
- Tukerman DB, Pease RFW. High performance heat sinking for VLSI. *IEEE Electron Devices Lett*. 1981;2(5):126–9.
- Hajmohammadi MR, Nourazar SS, Campo A. Analytical solution for two-phase flow between two rotating cylinders filled with power law liquid and a micro layer of gas. *J Mech Sci Technol*. 2014;28:1849–54.
- Ansari D, Husain A, Kim KY. Multi-objective optimization of a grooved micro-channel heat sink. *IEEE Trans Compon Packag Technol*. 2010;33(4):767–76.
- Hung T, Huang YX, Sheu TS, Yan WM. Numerical optimization of the thermal performance of a porous microchannel heat sink. *Numer Heat Transf Part A Appl*. 2014;65(5):1–16.
- Kulkarni K, Afzal A, Kim KY. Multi-objective optimization of a double-layered microchannel heat sink with temperature-dependent fluid properties. *Appl Therm Eng*. 2016;99:262–72.
- Husain A, Kim KY. Microchannel heat sink with designed roughness: analysis and optimization. *J Thermophys Heat Transf*. 2008;22(3):342–51.
- Husain A, Kim KY. Enhanced multi-objective optimization of a microchannel heat sink through evolutionary algorithm coupled with multiple surrogate models. *Appl Therm Eng*. 2010;30(13):1683–91.
- Xie G, Chen Z, Sunden B, Zhang W. Comparative study of the flow and thermal performance of liquid-cooling parallel-flow and counter-flow double-layer wavy microchannel heat sinks. *Numer Heat Transf Part A Appl*. 2013;64(1):30–55.
- Seyf HR, Nikaein B. Analysis of Brownian motion and particle-size effects on the thermal behavior and cooling performance of microchannel heat sinks. *Int J Therm Sci*. 2012;58:36–44.
- Wu JM, Zhao JY, Tseng K. Parametric study on the performance of double-layered microchannels heat sink. *Energy Convers Manag*. 2014;80:550–60.
- Chein R, Chuang J. Experimental microchannel heat sink performance studies using nanofluids. *Int J Therm Sci*. 2006;46:57–67.
- Jang SP, Choi S. Cooling performance of a microchannel heat sink with nanofluids. *Appl Therm Eng*. 2006;26:2457–63.
- Sui Y, Teo CJ, Lee PS, Chew YT, Shu C. Fluid flow and heat transfer in wavy microchannels. *Int J Heat Mass Transf*. 2010;53:2760–72.
- Ho CJ, Wei LC, Li ZW. An experimental investigation of forced convective cooling performance of a microchannel heat sink with Al_2O_3 /water nanofluid. *Appl Therm Eng*. 2010;30:96–103.
- Akbarinia A, Abdolzadeh M, Laur R. Critical investigation of heat transfer enhancement using nanofluids in microchannels with slip and non-slip flow regimes. *Appl Therm Eng*. 2011;31:556–65.
- Mah WH, Hung YM, Guo N. Entropy generation of viscous dissipative nanofluid flow in microchannels. *Int J Heat Mass Transf*. 2012;55:4169–82.
- Safaei MR, Gooarzi M, Akbari OA, Safdari Shadloo M, Dahari M. Performance evaluation of nanofluids in an inclined ribbed microchannel for electronic cooling applications. In: Murshed SMS, editor. *Electronics cooling*. In Tech; 2016. doi:10.5772/62898. <http://www.intechopen.com/books/electronics-cooling/performance-evaluation-of-nanofluids-in-an-inclined-ribbed-microchannel-for-electronic-cooling-appli>.
- Karimipour A, Alipour H, Akbari OA, Semiromi DT, Esfe MH. Studying the effect of indentation on flow parameters and slow heat transfer of water–silver nanofluid with varying volume fraction in a rectangular two-dimensional microchannel. *Ind J Sci Technol*. 2015;8(15):51707.
- Akbari OA, Toghraie D, Karimipour A. Numerical simulation of heat transfer and turbulent flow of water nanofluids copper oxide in rectangular microchannel with semi attached rib. *Adv Mech Eng*. 2016;8(4):1–25.
- Esfahani JA, Safaei MR, Goharimanesh M, Oliveira LR, Goodarzi M, Shamshirband Sh, Filho EPB. Comparison of experimental data, modelling and non-linear regression on transport properties of mineral oil based nanofluids. *Powder Technol*. 2017;317:458–70.
- Safaei MR, Safdari Shadloo M, Goodarzi MS, Hadjadj A, Goshayeshi HR, Afrand M, Kazi SN. A survey on experimental and numerical studies of convection heat transfer of nanofluids inside closed conduits. *Adv Mech Eng*. 2016;8(10):1–14.
- Safaei MR, Ahmadi G, Goodarzi MS, Safdari Shadloo M, Goshayeshi HR, Dahari M. Heat transfer and pressure drop in fully developed turbulent flow of graphene nanoplatelets–silver/water nanofluids. *Fluids*. 2016;1(3):1–20.

29. Goshayeshi HR, Safaei MR, Goodarzi M, Dahari M. Particle size and type effects on heat transfer enhancement of ferro-nanofluids in a pulsating heat pipe under magnetic field. *Powder Technol.* 2016;301:1218–26.
30. Safaei MR, Ahmadi G, Goodarzi MS, Kamyar A, Kazi SN. Boundary layer flow and heat transfer of FMWCNT/water nanofluids over a flat plate. *Fluids.* 2016;1(4):1–13.
31. Goshayeshi HR, Goodarzi M, Dahari M. Effect of magnetic field on the heat transfer rate of kerosene/Fe₂O₃ nanofluid in a copper oscillating heat pipe. *Exp Therm Fluid Sci.* 2015;68:663–8.
32. Goodarzi M, Kherbeet AS, Afrand M, Sadeghinezhad E, Mehrali M, Zahedi P, Wongwises S, Dahari M. Investigation of heat transfer performance and friction factor of a counter-flow double-pipe heat exchanger using nitrogen-doped, graphene-based nanofluids. *Intl Commun Heat Mass Transf.* 2016;76:16–23.
33. Safaei MR, Togun H, Vafai K, Kazi SN, Badarudin A. Investigation of heat transfer enhancement in a forward-facing contracting channel using FMWCNT nanofluids. *Numer Heat Transf Part A Appl.* 2014;66:1321–40.
34. Goshayeshi HR, Goodarzi M, Safaei MR, Dahari M. Experimental study on the effect of inclination angle on heat transfer enhancement of a ferro-nanofluid in a closed loop oscillating heat pipe under magnetic field. *Exp Therm Fluid Sci.* 2016;74:265–70.
35. Safaei MR, Jahanbin AH, Kianifar A, Gharehkhani S, Kherbeet AS, Goodarzi M, Dahari M. Mathematical modeling for nanofluids simulation: a review of the latest works. In: Akbar NS, editor. *modeling and simulation in engineering sciences.* InTech; 2016. doi:10.5772/64154. <http://www.intechopen.com/books/modeling-and-simulation-in-engineering-sciences/mathematical-modeling-for-nanofluids-simulation-a-review-of-the-latest-works>.
36. Nikkhab Z, Karimipour A, Safaei MR, Forghani-Tehrani P, Goodarzi M, Dahari M, Wongwises S. Forced convective heat transfer of water/functionalized multi-walled carbon nanotube nanofluids in a microchannel with oscillating heat flux and slip boundary condition. *Int Commun Heat Mass Transf.* 2015;68:69–77.
37. Khan WA, Khan ZH, Rahi M. Fluid flow and heat transfer of carbon nanotubes along a flat plate with Navier slip boundary. *Appl Nanosci.* 2014;4:633–41.
38. Leng C, Wang XD, Wang TH. An improved design of double-layered microchannel heat sink with truncated top channels. *Appl Therm Eng.* 2015;79:54–62.
39. Raisi A, Ghasemi B, Aminossadati SM. A numerical study on the forced convection of laminar nanofluid in a microchannel with both slip and no slip condition. *Numer Heat Transf A Appl.* 2011;59:114–29.
40. Akbari OA, Karimipour A, Semiromi DT, Safaei MR, Alipour H, Goodarzi M, Dahari M. Investigation of Rib's height effect on heat transfer and flow parameters of laminar water Al₂O₃ nanofluid in a two dimensional Rib-microchannel. *Appl Math Comput.* 2016;290:135–53.
41. Islami SB, Dastvareh B, Gharraei R. An investigation on the hydrodynamic and heat transfer of nanofluid flow with non-Newtonian base fluid, in micromixers. *Int J Heat Mass Transf.* 2014;78:917–29.
42. Akbari OA, Toghraie D, Karimipour A, Marzban A, Ahmadi GR. The effect of velocity and dimension of solid nanoparticles on heat transfer in non-Newtonian nanofluid. *Physica E.* 2017;86:68–75.
43. Derakhshan MM, Akhavan-Behabadi MA. Mixed convection of MWCNT-heat transfer oil nanofluid inside inclined plain and microfin tubes under laminar assisted flow. *Int J Therm Sci.* 2016;99:1–8.
44. Xia GD, Liu R, Wang J, Du M. The characteristics of convective heat transfer in microchannel heat sinks using Al₂O₃ and TiO₂ nanofluids. *Int Commun Heat Mass Transf.* 2016;76:256–64.
45. Leng C, Wang XD, Wang TH, Yan WM. Multi-parameter optimization of flow and heat transfer for a novel double-layered microchannel heat sink. *Int J Heat Mass Transf.* 2015;84:359–69.
46. Akbari OA, Toghraie D, Karimipour A. Impact of ribs on flow parameters and laminar heat transfer of water–aluminum oxide nanofluid with different nanoparticle volume fractions in a three-dimensional rectangular microchannel. *Adv Mech Eng.* 2015;7(11):1–11.
47. Akbari OA, Goodarzi M, Safaei MR, Zarringhalam M, Ahmadi GR, Dahari M. A modified two-phase mixture model of nanofluid flow and heat transfer in 3-D curved microtube. *Adv Powder Technol.* 2016;27:2175–85.
48. Alipour H, Karimipour A, Safaei MR, Semiromi DT, Akbari OA. Influence of T-semi attached rib on turbulent flow and heat transfer parameters of a silver–water nanofluid with different volume fractions in a three-dimensional trapezoidal microchannel. *Physica E.* 2017;88:60–76.
49. Behnampour A, Akbari OA, Safaei MR, Ghavami M, Marzban A, Ahmadi Sheikh Shabani GR, Zarringhalam M, Mashayekhi R. Analysis of heat transfer and nanofluid fluid flow in microchannels with trapezoidal, rectangular and triangular shaped ribs. *Physica E.* 2017;9:15–31.
50. Akbari OA, Afrouzi HH, Marzban A, Toghraie D, Malekzade H, Arabpour A. Investigation of volume fraction of nanoparticles effect and aspect ratio of the twisted tape in the tube. *J Therm Anal Calorim.* 2017;. doi:10.1007/s10973-017-6372-7.
51. Esfe MH, Afrand M, Yan WM, Yarmand H, Toghraie D, Dahari M. Effects of temperature and concentration on rheological behavior of MWCNTs/SiO₂ (20–80)-SAE40 hybrid nano-lubricant. *Int Commun Heat Mass Transf.* 2016;76:133–8.
52. Esfe MH, Ahangar MRH, Rejvani M, Toghraie D, Hajmohammad MH. Designing an artificial neural network to predict dynamic viscosity of aqueous nanofluid of TiO₂ using experimental data. *Int Commun Heat Mass Transf.* 2016;75:192–6.
53. Afrand M, Toghraie D, Sina N. Experimental study on thermal conductivity of water-based Fe₃O₄ nanofluid: development of a new correlation and modeled by artificial neural network. *Int Commun Heat Mass Transf.* 2016;75:262–9.
54. Aminossadati SM, Raisi A, Ghasemi B. Effects of magnetic field on nanofluid forced convection in a partially heated microchannel. *Int J Non-Linear Mech.* 2011;46:1373–82.
55. Afrand M, Sina N, Teimouri H, Mazaheri A, Safaei MR, Esfe MH, Kamali J, Toghraie D. Effect of magnetic field on free convection in inclined cylindrical annulus containing molten potassium. *Int J Appl Mech.* 2015;7(04):1550052.
56. Noorian H, Toghraie D, Azimian AR. Molecular dynamics simulation of Poiseuille flow in a rough nano channel with checker surface roughnesses geometry. *Heat Mass Transf.* 2014;50(1):105–13.
57. Zarringhalam M, Karimipour A, Toghraie D. Experimental study of the effect of solid volume fraction and Reynolds number on heat transfer coefficient and pressure drop of CuO–water nanofluid. *Exp Therm Fluid Sci.* 2016;76:342–51.
58. Toghraie D, Azimian AR. Molecular dynamics simulation of liquid–vapor interface on the solid surface using the GEAR'S algorithm. *Dynamics.* 2009;182:15493.
59. Semiromi DT, Azimian AR. Molecular dynamics simulation of nonodroplets with the modified Lennard–Jones potential function. *Heat Mass Transf.* 2010;47:579–88.
60. Semiromi DT, Azimian AR. Nanoscale Poiseuille flow and effects of modified Lennard–Jones potential function. *Heat Mass Transf.* 2010;46:791–801.

61. Semiromi DT, Azimian AR. Molecular dynamics simulation of liquid–vapor phase equilibrium by using the modified Lennard–Jones potential function. *Heat Mass Transf.* 2010;46:287–94.
62. Sajadifar SA, Karimipour A, Toghraie D. Fluid flow and heat transfer of non-Newtonian nanofluid in a microtube considering slip velocity and temperature jump boundary conditions. *Eur J Mech B Fluid.* 2017;61:25–32.
63. Rezaei M, Azimian AR, Semiromi DT. The surface charge density effect on the electro-osmotic flow in a nanochannel: a molecular dynamics study. *Heat Mass Transf.* 2015;51:661–70.
64. Rezaei M, Azimian AR, Toghraie D. Molecular dynamics study of an electro-kinetic fluid transport in a charged nanochannel based on the role of the stern layer. *Physica A Stat Mech Appl.* 2015;426:25–34.
65. Oveissi S, Eftekhari SA, Toghraie D. Longitudinal vibration and instabilities of carbon nanotubes conveying fluid considering size effects of nanoflow and nanostructure. *Physica E Low Dimens Syst Nanostruct.* 2016;83:164–73.
66. Oveissi S, Toghraie D, Eftekhari SA. Longitudinal vibration and stability analysis of carbon nanotubes conveying viscous fluid. *Physica E Low Dimens Syst Nanostruct.* 2016;83:275–83.
67. Noorian H, Toghraie D, Azimian AR. The effects of surface roughness geometry of flow undergoing Poiseuille flow by molecular dynamics simulation. *Heat Mass Transf.* 2014;50:95–104.
68. Nazari S, Toghraie D. Numerical simulation of heat transfer and fluid flow of water–CuO Nanofluid in a sinusoidal channel with a porous medium. *Physica E Low Dimens Syst Nanostruct.* 2017;87:134–40.
69. Esfe MH, Akbari M, Semiromi DT, Karimipour A, Afrand M. Effect of nanofluid variable properties on mixed convection flow and heat transfer in an inclined two-sided lid-driven cavity with sinusoidal heating on sidewalls. *Heat Transf Res.* 2014;45(5):409–432.
70. Esfe MH, Arani AAA, Karimipour A, Esforjani SSM. Numerical simulation of natural convection around an obstacle placed in an enclosure filled with different types of nanofluids. *Heat Transf Res.* 2014;45(3):279–292.
71. Esfe MH, Esforjani SSM, Akbari M, Karimipour A. Mixed-convection flow in a lid-driven square cavity filled with a nanofluid with variable properties: effect of the nanoparticle diameter and of the position of a hot obstacle. *Heat Transf Res.* 2014;45(6):563–578.
72. Zadkhan M, Toghraie D, Karimipour A. Developing a new correlation to estimate the thermal conductivity of MWCNT–CuO/water hybrid nanofluid via an experimental investigation. *J Therm Anal Calorim.* 2017;. doi:10.1007/s10973-017-6213-8.
73. Esfe MH, Naderi A, Akbari M, Afrand M, Karimipour A. Evaluation of thermal conductivity of COOH-functionalized MWCNTs/water via temperature and solid volume fraction by using experimental data and ANN methods. *J Therm Anal Calorim.* 2015;121(3):1273–8.
74. Afrand M. Experimental study on thermal conductivity of ethylene glycol containing hybrid nano-additives and development of a new correlation. *Appl Therm Eng.* 2017;110:1111–9.
75. Eshgarf H, Afrand M. An experimental study on rheological behavior of non-Newtonian hybrid nano-coolant for application in cooling and heating systems. *Exp Therm Fluid Sci.* 2016;76:221–7.
76. Shareghi S, Toghraie D. Numerical simulation of blood flow in healthy arteries by use of the sisko model. *Comput Therm Sci Int J.* 2016;8(4).
77. Mirmasoumi S, Behzadmehr A. Numerical study of laminar mixed convection of a nanofluid in a horizontal tube using two-phase mixture model. *Appl Therm Eng.* 2008;28:717–27.
78. Soltanimehr M, Afrand M. Thermal conductivity enhancement of COOH functionalized MWCNTs/ethylene glycol–water nanofluid for application in heating and cooling systems. *Appl Therm Eng.* 2016;105:716–23.
79. Afrand M, Najafabadi KN, Akbari M. Effects of temperature and solid volume fraction on viscosity of SiO₂–MWCNTs/SAE40 hybrid nanofluid as a coolant and lubricant in heat engines. *Appl Therm Eng.* 2016;102:45–54.
80. Oveisi S, Nahvi H, Toghraie D. Investigation of dynamical behavior (transverse vibration) and instability analysis of carbon nanotubes conveying nanofluid. *J Solid Mech Eng.* 2013;6:15–23.
81. Afrand M, Farahat S, Nezhad AH, Sheikhzadeh GA, Sarhaddi F. Numerical simulation of electrically conducting fluid flow and free convective heat transfer in an annulus on applying a magnetic field. *Heat Transf Res.* 2014;45(8):749–66.
82. Esfe MH, Refahi AH, Teimouri H, Javad Noroozi M, Afrand M, Karimipour A. Mixed convection fluid flow and heat transfer of the Al₂O₃–water nanofluid with variable properties in a cavity with an inside quadrilateral obstacle. *Heat Transf Res.* 2015;46(5):465–482.
83. Jafarmadar S, Azizinia N, Razmara N, Mobadersani F. Thermal analysis and entropy generation of pulsating heat pipes using nanofluids. *Appl Therm Eng.* 2016;103:356–64.
84. Esfe MH, Karimipour A, Yan WM, Akbari M, Safaei MR, Dahari M. Experimental study on thermal conductivity of ethylene glycol based nanofluids containing Al₂O₃ nanoparticles. *Int J Heat Mass Transf.* 2015;88:728–34.
85. Afrand M, Rostami S, Akbari M, Wongwises S, Esfe MH, Karimipour A. Effect of induced electric field on magneto-natural convection in a vertical cylindrical annulus filled with liquid potassium. *Int J Heat Mass Transf.* 2015;90:418–26.
86. Afrand M, Toghraie D, Karimipour A, Wongwises S. A numerical study of natural convection in a vertical annulus filled with gallium in the presence of magnetic field. *J Magnet Magn Mater.* 2017;430:22–8.
87. Esfe MH, Wongwises S, Naderi A, Asadi A, Safaei MR, Rostamian H, Dahari M, Karimipour A. Thermal conductivity of Cu/TiO₂–water–EG hybrid nanofluid: experimental data and modeling using artificial neural network and correlation. *Int Commun Heat Mass Transf.* 2015;66:100–4.
88. Safaei MR, Mahian O, Garoosi F, Hooman K, Karimipour A, Kazi SN, Gharekhani S. Investigation of micro and nano-sized particle erosion in a 90° pipe bend using a two-phase discrete phase model. *Sci World J.* 2014;2014, 740578.
89. Afrand M. Using a magnetic field to reduce natural convection in a vertical cylindrical annulus. *Int J Therm Sci.* 2017;118:12–23.
90. Afrand M, Farahat S, Nezhad AH, Sheikhzadeh GhA, Sarhaddi F, Wongwises S. Multi-objective optimization of natural convection in a cylindrical annulus mold under magnetic field using particle swarm algorithm. *Int Commun Heat Mass Transf.* 2015;60:13–20.
91. Afrand M, Farahat S, Nezhad AH, Sheikhzadeh GA, Sarhaddi F. 3-D numerical investigation of natural convection in a tilted cylindrical annulus containing molten potassium and controlling it using various magnetic fields. *Int J Appl Electromagn Mech.* 2014;46(4):809–21.
92. Karimipour A, Taghipour A, Malvandi A. Developing the laminar MHD forced convection flow of water/FMWNT carbon nanotubes in a microchannel imposed the uniform heat flux. *J Magn Magn Mater.* 2016;419:420–8.
93. Goodarzi M, Amiri A, Goodarzi MS, Safaei MR, Karimipour A, Languri EM, Dahari M. Investigation of heat transfer and pressure drop of a counter flow corrugated plate heat exchanger using MWCNT based nanofluids. *Int Commun Heat Mass Transf.* 2015;66:172–9.

94. Karimipour A, Nezhad AH, D'Orazio A, Shirani E. Investigation of the gravity effects on the mixed convection heat transfer in a microchannel using lattice Boltzmann method. *Int J Therm Sci.* 2012;54:142–52.
95. Karimipour A, Afrand M. Magnetic field effects on the slip velocity and temperature jump of nanofluid forced convection in a microchannel. *Proc Inst Mech Eng Part C J Mech Eng Sci.* 2016;230(1):1921–36.
96. Karimipour A, Esfe MH, Safaei MR, Semiromic DT, Jafari S, Kazi SN. Mixed convection of copper–water nanofluid in a shallow inclined lid driven cavity using the lattice Boltzmann method. *Physica A.* 2014;402:150–68.
97. Karimipour A, Nezhad AH, D'Orazio A, Esfe MH, Safaei MR, Shirani E. Simulation of copper–water nanofluid in a microchannel in slip flow regime using the lattice Boltzmann method. *Eur J Mech B Fluids.* 2015;49:89–99.
98. Afrand M, Toghraie D, Ruhani B. Effects of temperature and nanoparticles concentration on rheological behavior of Fe₃O₄–Ag/EG hybrid nanofluid: an experimental study. *Exp Therm Fluid Sci.* 2016;77:38–44.
99. Karimipour A. New correlation for Nusselt number of nanofluid with Ag/Al₂O₃/Cu nanoparticles in a microchannel considering slip velocity and temperature jump by using lattice Boltzmann method. *Int J Therm Sci.* 2015;91:146–56.
100. Esfe MH, Yan WM, Afrand M, Sarraf M, Toghraie D, Dahari M. Estimation of thermal conductivity of Al₂O₃/water (40%)–ethylene-glycol (60%) by artificial neural network and correlation using experimental data. *Int Commun. Heat Mass Transf.* 2016;74:125–8.
101. Karimipour A, Nezhad AH, Behzadmehr A, Alikhani S, Abedini E. Periodic mixed convection of a nanofluid in a cavity with top lid sinusoidal motion. *Proc Inst Mech Eng Part C J Mech Eng Sci.* 2011;225(9):2149–60.
102. Toghraie D, Chaharsoghi VA, Afrand M. Measurement of thermal conductivity of ZnO–TiO₂/EG hybrid nanofluid. *J Therm Anal Calorim.* 2016; doi:10.1007/s10973-016-5436-4.
103. Esfe MH, Saedodin S, Asadi A, Karimipour A. Thermal conductivity and viscosity of Mg (OH) 2-ethylene glycol nanofluids. *J Therm Anal Calorim.* 2015;120(2):1145–9.
104. Toghraie D, Alempour SMB, Afrand M. Experimental determination of viscosity of water based magnetite nanofluid for application in heating and cooling systems. *J Magn Magn Mater.* 2016;417:243–8.
105. Harandi SS, Karimipour A, Afrand M, Akbari M, D'Orazio A. An experimental study on thermal conductivity of F-MWCNTs–Fe₃O₄/EG hybrid nanofluid: effects of temperature and concentration. *Int Commun Heat Mass Transf.* 2016;76:171–7.
106. Esfe MH, Afrand M, Gharehkhani S, Rostamian H, Toghraie D, Dahari M. An experimental study on viscosity of alumina-engine oil: effects of temperature and nanoparticles concentration. *Int Commun Heat Mass Transf.* 2016;76:202–8.
107. Heydari M, Toghraie D, Akbari OA. The effect of semi-attached and offset mid-truncated ribs and water/TiO₂ nanofluid on flow and heat transfer properties in a triangular microchannel. *Therm Sci Eng Prog.* 2017;2:140–50.
108. Shamsi MR, Akbari OA, Marzban A, Toghraie D, Mashayekhi R. Increasing heat transfer of non-Newtonian nanofluid in rectangular microchannel with triangular ribs. *Physica E.* 2017;93:167–78.
109. Khodabandeh E, Rahbari A, Rosen MA, Ashrafi ZN, Akbari OA, Anvari AM. Experimental and numerical investigations on heat transfer of a watercooled lance for blowing oxidizing gas in an electrical arc furnace. *Energ Convers Manag.* 2017;148:43–56.
110. Arani AAA, Akbari OA, Safaei MR, Marzban A, Alrashed AAAA, Ahmadi GR, Nguyen TK. Heat transfer improvement of water/single-wall carbon nanotubes (SWCNT) nanofluid in a novel design of a truncated double layered microchannel heat sink. *Int J Heat Mass Transf.* 2017;113:780–95.
111. Rezaei O, Akbari OA, Marzban A, Toghraie D, Pourfattah F, Mashayekhi R. The numerical investigation of heat transfer and pressure drop of turbulent flow in a triangular microchannel. *Physica E.* 2017;93:179–89.
112. Gravndyan Q, Akbari OA, Toghraie D, Marzban A, Mashayekhi R, Karimi R, Pourfattah F. The effect of aspect ratios of rib on the heat transfer and laminar water/TiO₂ nanofluid flow in a two-dimensional rectangular microchannel. *J Mol Liq.* 2017;236:254–65.
113. Kherbeet AS, Safaei MR, Mohammed HA, Salman BH, Ahmed HE, Alawi OA, Al-Asadi MT. Heat transfer and fluid flow over microscale backward and forward facing step: a review. *Int Commun Heat Mass Transf.* 2016;76:237–44.
114. Baratpour M, Karimipour A, Afrand M, Wongwises S. Effects of temperature and concentration on the viscosity of nanofluids made of single-wall carbon nanotubes in ethylene glycol. *Int Commun Heat Mass Transf.* 2016;74:108–13.
115. Ahmadi GR, Toghraie D, Azimian A, Akbari OA. Evaluation of synchronous execution of full repowering and solar assisting in a 200 mw steam power plant, a case study. *Appl Therm Eng.* 2017;112:111–23.
116. Ahmadi GR, Akbari OA, Zarringhalam M. Energy and exergy analyses of partial repowering of a natural gas-fired steam power plant. *Int J Exergy.* 2017;23(2):149–68.
117. Akbari OA, Marzban A, Ahmadi GR. Evaluation of supply boiler repowering of an existing natural gas-fired steam power plant. *Appl Therm Eng.* 2017;124:897–910.
118. Ahmadi GR, Toghraie D, Akbari OA. Solar parallel feed water heating repowering of a steam power plant: a case study in Iran. *Renew Sustain Energy Rev.* 2017;77:474–85.
119. Ahmadi GR, Toghraie D. Energy and exergy analysis of Montazeri steam power plant in Iran. *Renew Sustain Energy Rev.* 2016;56:454–63.
120. Ahmadi GR, Toghraie D, Akbari OA. Efficiency improvement of a steam power plant through solar repowering. *Int J Exergy.* 2017;22(2):158–82.